THREE-DIMENSIONAL DNS OF METHANE-AIR TURBULENT PREMIXED FLAMES WITH REALISTIC REDUCED KINETIC MECHANISM

Mamoru Tanahashi, Satoshi Kikuta, Nobuhiro Shiwaku, Toshio Miyauchi
Department of Mechanical and Aerospace Engineering,
Tokyo Institute of Technology
2-12-1 Ookayama, Meguro-ku, Tokyo 152-8850, Japan
mtanahas@mes.titech.ac.jp, sakikuta@navier.mes.titech.ac.jp,
nshiwaku@navier.mes.titech.ac.jp, tmiyauch@mes.titech.ac.jp

Yuzuru Nada
Faculty of Risk and Crisis Management,
Chiba Institute of Science
3 Shiomi-cho, Choshi-city, Chiba 288-0025, Japan
ynada@cis.ac.jp

ABSTRACT

Three-dimensional direct numerical simulations (DNS) of methane-air turbulent premixed flames with a realistic reduced kinetic mechanism have been conducted to investigate effects of turbulence characteristics on the local flame structure. The reduced kinetic mechanism (MeCH-19), which is constructed based on GRI Mech. 2.11, is verified by comparing with two detailed kinetic mechanisms; GRI Mech. 2.11 and Miller & Bowman through the two-dimensional DNS. Important properties such as temperature, heat release rate and turbulent burning velocity obtained from detailed and reduced kinetic mechanisms are compared and they show good agreements with each other. Since the availability of MeCH-19 is verified by two-dimensional DNS, three-dimensional DNS is conducted using MeCH-19. Numerical conditions of the DNS can be classified into thin reaction zones. Different from our previous DNSs of hydrogen-air turbulent premixed flames, the distributions of temperature and heat release rate do not coincide and quite low heat release rate regions corresponding to the local extinction are observed. In the vicinities of these regions, flame elements are strongly stretching into two tangential directions. The local extinction mechanism was clarified by introducing lifetime of reactive species relative to eddy turnover time of strong coherent fine scale eddies in turbulence.

INTRODUCTION

The characteristics of the turbulent premixed flames have been classified by the ratio of the laminar burning velocity (S_L) to turbulence intensity (u'_{rms}) and the ratio of the laminar flame thickness (δ_F) to turbulence length scale (l) (Borghi, 1985; Peters, 1986; 1999). Peters (1999) has proposed the combustion diagram based on the relation between u'_{rms}/S_L and l/δ_F, and has classified the flame structure into four regimes; wrinkled flamelets, corrugated flamelets, thin reaction zones and broken reaction zones. In the wrinkled and the corrugated flamelets regime, flame structure is considered to be approximated by the laminar flame with small curvature under strain field, whereas characteristics of the flame elements in the thin reaction zones and the broken reaction zones are supposed to be quite different from that of laminar flame. However, actual flame structures in each regime have not been clarified yet.

Due to the recent remarkable development of the computer technology, direct numerical simulations (DNS) of turbulent combustion with detailed kinetic mechanisms and temperature dependence of transport and thermal properties become possible (Baum et al., 1994a; Poinsot et al., 1996; Tanahashi et al., 1998; Hilbert et al., 2003). DNS of turbulent combustion with detailed kinetic mechanism have been extended to three-dimensional flow field for hydrogen fuel (Tanahashi et al., 2000; 2002; Nada et al., 2004a). From three-dimensional DNS of hydrogen-air turbulent premixed flames with a detailed kinetic mechanism, Tanahashi et al. (2000) have shown that coherent fine scale eddies of which mean diameter is about 8 times Kolmogorov length and maximum azimuthal velocity is about 1.2 times Kolmogorov velocity (Tanahashi et al., 1999; 2001; 2004) are very important for the determination of the local flame structure in turbulence. Three-dimensional flame structures are caused by strong fine scale eddies in turbulence and the handgrip and spire structures (Nada et al., 2004a) are observed even in the corrugated flamelets regime, and enhance flame wrinkling and local heat release rate.

It is well known that responses of flame structure to flow field such as strain rate are different for fuels. To investigate turbulent flame structure in details, three-dimensional DNS of hydrocarbon fuels are required. For hydrocarbons, several tens species and several hundreds elementary reactions have to be taken into account in DNS. DNS of turbulent combustion have been extended to hydrocarbon fuels such as methane and propane from simple hydrogen fuel (Echekki and Chen, 1996; Chen et al., 1998; Saito et al., 2002). However, almost all previous studies were restricted to two-dimensional calculations due to the limitation of computer resources. To realize three-dimensional DNS, high accurate reduced kinetic mechanisms, which are available for turbulent combustion, should be developed. In this study, three-dimensional DNS of methane-air turbulent premixed flames are conducted with a reduced kinetic mechanism to investigate fuel effects on the local flame

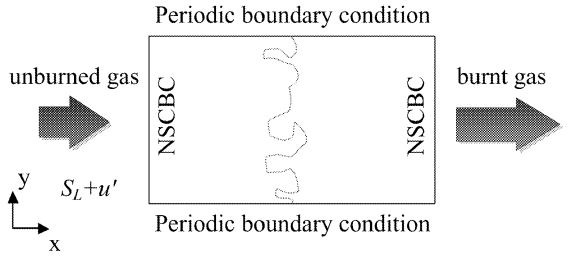

Figure 1: Geometry of the flow field.

Table 1: Numerical parameters for two-dimensional DNSs of methane-air turbulent premixed flames.

	Re_λ	Re_l	u'/S_L	l/δ_L
GRI Mech. 2.11	116	350	18.5	2.51
M&B	116	350	16.2	2.56
MeCH-19	116	350	18.4	2.52

structures and local extinction mechanism of premixed flames in high intensity turbulence. First, two-dimensional DNS with two different detailed kinetic mechanisms and a reduced kinetic mechanism were conducted to validate performance of a reduced kinetic mechanism for DNS of turbulent combustion. The validated reduced kinetic mechanism is applied for three-dimensional DNS and the results are analysed to investigate effect of fuel on the local flame structures and local extinction mechanism of turbulent premixed flames.

VALIDATION OF REDUCED KINETIC MECHANISM

Details of the governing equations can be found in Miyauchi et al. (1996). For detailed kinetic mechanisms, GRI Mech. 2.11 (49 reactive species and 279 elementary reactions) (Bowman et al.) and Miller & Bowman (51 reactive species and 235 elementary reactions) (Miller and Bowman, 1989) are used and, for a reduced kinetic mechanism, MeCH-19 (23 reactive species and 19 step reactions) (Homma, 2001) is used. The reactive species included in MeCH-19 are H_2, H, O, O_2, OH, H_2O, HO_2, C, CH_3, CH_4, CO, CO_2, CH_2O, C_2H_2, C_2H_4, C_2H_6, NH_3, NO, NO_2, HCN, HCNO, HNCO and N_2. The temperature dependence of the viscosity, the thermal conductivity and the diffusion coefficients are taken into account by linking CHEMKIN packages (Kee et al., 1986; 1989) with modifications for vector/parallel computations. Figure 1 shows a schematic of the flow field in the two-dimensional DNSs. The governing equations are discretized by 4th-order central difference scheme in the x direction and by a Fourier spectral method in the y direction. The boundary conditions in the x direction are NSCBC (Poinsot and Lele, 1992; Baum et al., 1994b) and those in the y direction are periodic. Time integration is implemented by the third-order Runge-Kutta scheme.

Numerical parameters of DNSs are listed in Table 1. The initial turbulent velocity fields are same in all cases. A methane-air mixture in the unburned side is set to $\phi = 1.0$ at 0.1MPa and 700K. The inflow boundary condition for the velocity field is given as $u_{in} = S_L + u'(y,t)$. The turbulence $u'(y,t)$ was obtained by the preliminary DNS of homogeneous isotropic turbulence by a spectral method and Reynolds number based on Taylor micro scale Re_λ is 116.4. δ_L denotes laminar flame thickness based on temperature gradient and

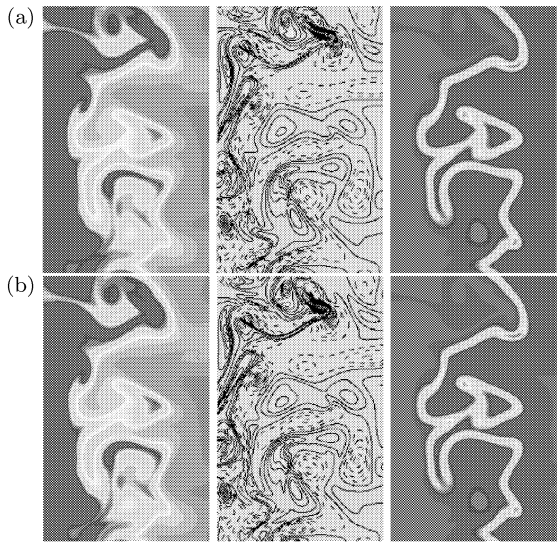

Figure 2: Distributions of temperature, vorticity and heat release rate obtained from two-dimensional DNS with GRI Mech. 2.11 (a) and MeCH-19 (b).

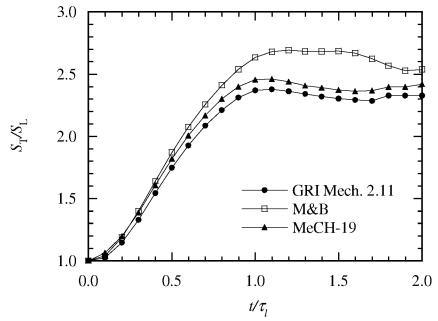

Figure 3: Temporal developments of turbulent burning velocities obtained from two-dimensional DNS with different kinetic mechanism.

is defined by $\delta_L = (T_b - T_u)/(\partial T/\partial x)_{max}$, where T_u and T_b denote temperature in the unburned and burned side, respectively.

Figure 2 shows distributions of temperature, vorticity and heat release rate obtained from GRI Mech. 2.11 and MeCH-19. The distributions of important properties obtained from MeCH-19 coincide very well with those obtained by GRI Mech. 2.11 except for the minor species which are calculated by the assumption of the steady state. Figure 3 shows temporal development of the turbulent burning velocity for three kinetic mechanisms. The burning velocity obtained by Miller & Bowman is a little bit high compared with GRI Mech. 2.11 and MeCH-19. This difference is caused by reaction rates related to CH_4 and inherent characteristics of the kinetic mechanism. These results suggest that MeCH-19 is available for DNS of turbulent premixed flames. The use of MeCH-19 reduces computational time and memory to about 1/8 and 1/2, respectively.

THREE DIMENSIONAL DNS OF METHANE-AIR TURBULENT PREMIXED FLAME

Since the availability of MeCH-19 is verified by the two-dimensional DNS, three-dimensional DNS of methane-air turbulent premixed flame is conducted with MeCH-19. Numerical methods are same as the two-dimensional DNSs. Boundary

Table 2: Numerical parameters for three-dimensional DNS of methane-air turbulent premixed flames.

Re_λ	Re_l	u'/S_L	l/δ_L	D/δ_L
37.4	144	5.80	3.28	0.75

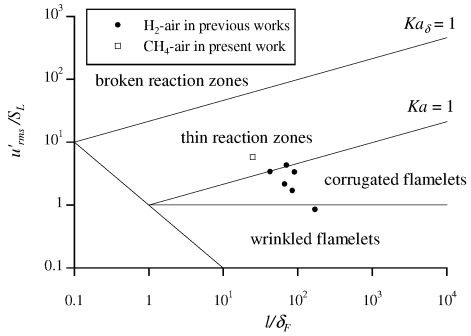

Figure 4: The location the three-dimensional DNS on the turbulent combustion diagram.

condition and spatial discretization in the z direction are periodic and Fourier spectral method, respectively. Inflow boundary condition for chemical species is set to be methane-air mixture with $\phi = 1.0$ at 0.1MPa and 950K. Computational domain is selected to be 5.5mm×5.5mm×5.5mm and $513 \times 192 \times 192$ grid points are used.

Table 2 shows the numerical parameters for the three-dimensional DNS of methane-air turbulent premixed flame. Fully-developed homogeneous isotropic turbulence of which Reynolds number based on Taylor micro scale is about 37.4 is used for initial and inflow boundary condition for the velocity field. Figure 4 shows the location of the present DNS and previous DNSs of hydrogen-air cases (Tanahashi et al., 2000; 2002; Nada et al., 2004a) on the turbulent combustion diagram of Peters (1999). The present DNS is classified into the thin reaction zones. D/δ_L in Table 2 denotes the ratio of the most expected diameter $D(= 8\eta)$ of the coherent fine scale eddies to the laminar flame thickness δ_L. In our previous study (Tanahashi et al., 2000), it has been shown that the coherent fine scale eddies in turbulence play important roles in the local flame structure of the turbulent premixed flames.

FLAME STRUCTURE OF METHANE-AIR TURBULENT PREMIXED FLAME

Figure 5 shows contour surfaces of temperature (1400K) and heat release rate ($\Delta H/\Delta H_L = 1.0$) with distributions of axes of coherent fine scale eddies. Here ΔH_L denotes the maximum heat release rate of the laminar flame. Similar to the cases of hydrogen-air premixed flames, the coherent fine scale eddies existing in the vicinity of the flame fronts decay due to the increase of viscosity and the effect of expansion caused by temperature rise. Flame fronts are distorted by the fine scale eddies in the unburned side. However, differences between hydrogen-air and methane-air turbulent premixed flames can be observed in distribution of the heat release rate. In Fig. 5(b), there is a large region of low heat release rate (see circle in Fig. 5(b)). This has never been observed in hydrogen-air turbulent premixed flames even for the same turbulence intensity. Figure 6 shows distributions of temperature and heat

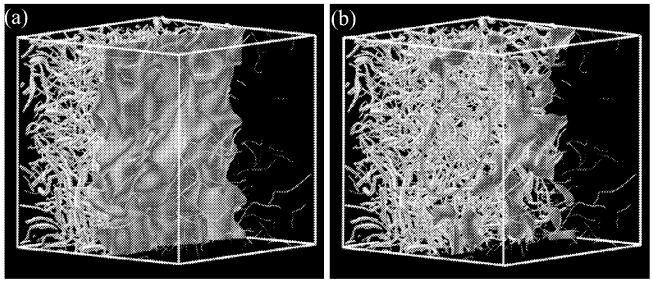

Figure 5: Contour surfaces of temperature (a) and heat release rate (b) with distributions of axes of coherent fine scale eddies.

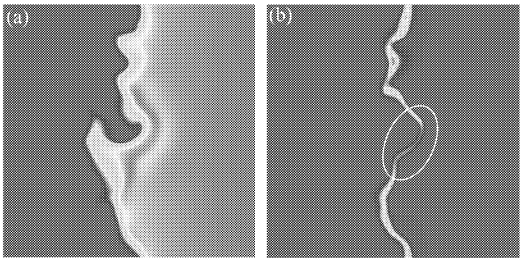

Figure 6: Distributions of temperature (a) and heat release rate (b) on a typical cross-section.

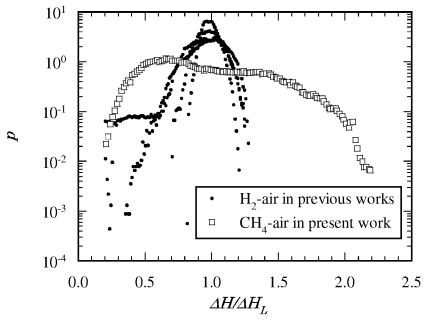

Figure 7: Provability density functions of local heat release rate of hydrogen-air and methane-air turbulent premixed flames.

release rate on the typical cross-section including the low heat release area. The low heat release rate area (see circle in Fig. 6(b)) shows about $0.3\Delta H_L$ although temperature is relatively uniform and still high. There is a possibility that this region represents the local extinction in turbulent premixed flames.

STATISTICAL CHARACTERISTICS OF LOCAL FLAME STRUCTURE

To clarify effects of turbulence characteristics on local flame structure quantitatively, the statistical characteristics of flame elements are investigated. The flame fronts are defined as points with the local maximum temperature gradient. Probability density functions of local heat release rate in methane-air and hydrogen-air turbulent premixed flames are shown in Fig. 7. The local heat release rate is the maximum heat release rate in a flame element and normalized by ΔH_L. The variance of local heat release rate in methane-air turbulent premixed flame is much larger than those in hydrogen-air turbulent premixed flames, and there are lots of flame elements that show high heat release rate of $2.0\Delta H_L$ and low heat release rate of

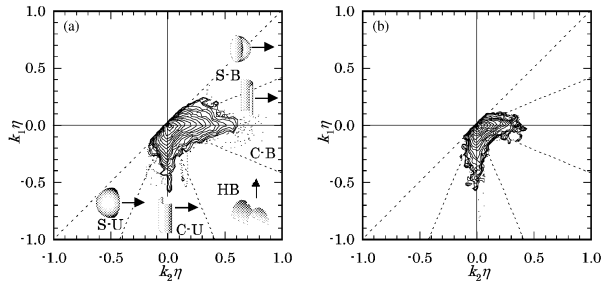

Figure 8: Joint probability density functions of principal curvatures of flame front for H_2-air flame in previous work (a) and for CH_4-air flame (b).

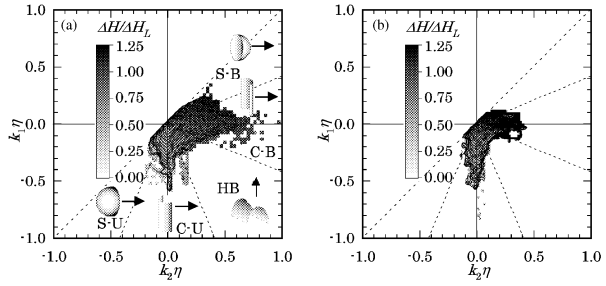

Figure 9: Mean heat release rates conditioned by principal curvatures for H_2-air flame in previous work (a) and for CH_4-air flame (b).

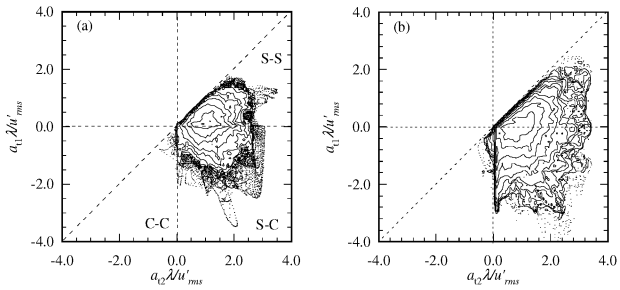

Figure 10: Joint probability density functions of tangential strain rates at flame front for H_2-air flame in previous work (a) and for CH_4-air flame (b).

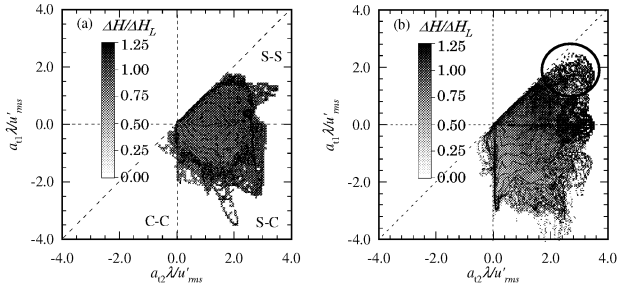

Figure 11: Mean heat release rates conditioned by tangential strain rate at the flame front for H_2-air flame in previous work (a) and for CH_4-air flame (b).

$0.5\Delta H_L$ along the flame front. For hydrogen-air turbulent premixed flames, probability density functions show their peaks at about $1.0\Delta H_L$. For methane-air turbulent premixed flame, however, probability density function shows a weak peak at $0.7\Delta H_L$. This value is lower than the maximum heat release rate of the laminar case.

In the previous study (Nada et al., 2004b), it is clarified that local heat release rates show strong correlation with three-dimensional geometrical shapes of the flame element in hydrogen-air turbulent premixed flames with $\phi = 1.0$. In this study, the correlation between local heat release rates and geometrical shapes of flame front is also examined by using principal curvatures (k_1 and k_2). Principal curvatures are defined as $k = k_1 + k_2 = 1/r_1 + 1/r_2 (k_1 < k_2)$, where k, r_1 and r_2 denote mean curvature and two radii of curvature of the flame surface, respectively. Figure 8 shows the joint probability density functions of principal curvatures of flame front for H_2-air flame and CH_4-air flame. The flame elements convex toward the burned side are defined to have positive value and the principal curvatures are normalized by Kolmogorov length (η). The probability difference between neighboring contour lines is 2.0 times. From the two principal curvatures, flame shape can be classified into spherical surface convex toward the burned side (S-B), cylindrical surface convex toward the burned side (C-B), hyperboloidal surface (HB), cylindrical surface convex toward the unburned side (C-U) and spherical surface convex toward the unburned side (S-U). In Fig. 8(a), typical shapes of flame elements in each regimes are shown schematically, where the arrows denote the burned side. Although flame elements in both cases are distributed in every regimes, the maximum value of $|k_2\eta|$ is smaller than that of $|k_1\eta|$ in the case of methane-air turbulent premixed flame. The curvatures of flame elements convex toward the burned side tend to be smaller than those of flame elements convex toward the unburned side. Figure 9 shows mean local heat release rates conditioned by k_1 and k_2. Heat release rates tend to decrease when the regime changes from S-B to S-U, while the correlation between heat release rate and curvatures for methane-air turbulent premixed flame is not clear compared with hydrogen-air case.

Similar to the of curvature, it is necessary to divide tangential strain rates into two components. The tangential strain rate can be split into the minimum tangential strain rate (a_{t1}) and the maximum tangential strain rate (a_{t2}). Figure 10 shows joint probability density functions of tangential strain rates at flame front for H_2-air flame and CH_4-air flame. Tangential strain rates are normalized by the time scale based on Taylor micro scale. Due to the conditions of the strain rate, flame elements can be classified into three regime; stretching-stretching (S-S), stretching-compression (S-C) and compression-compression (C-C) regime. Probabilities of flame elements that are affected by two-dimensional strain of the order of Taylor time scale are high in both cases, and almost all flame elements are stretched into one tangential direction at least. Figure 11 shows mean local heat release rates conditioned by a_{t1} and a_{t2}. In the cases of hydrogen-air turbulent premixed flames, correlations between heat release rates and tangential strain rates are hardly observed. However, in the case of methane-air turbulent premixed flame, they show relatively strong correlation. The heat release rates tend to increase from C-C regime to S-S regime. In S-S regime, the heat release rate also increases with increase of the tangential strain rate. However, in S-S regime, the flame elements that are stretching strongly in two directions (see circle in Fig. 11(b)) tend to show low heat release rate. Most of these flame elements exist in the vicinity of low heat release rate region in Fig. 5 and they are considered to be closely related to local extinction of turbulent premixed flames.

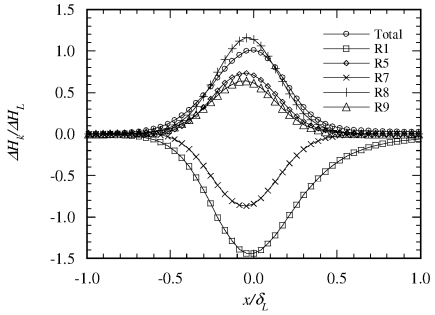

Figure 12: Contributions of dominant elementary reactions to heat release rate in methane-air laminar premixed flame.

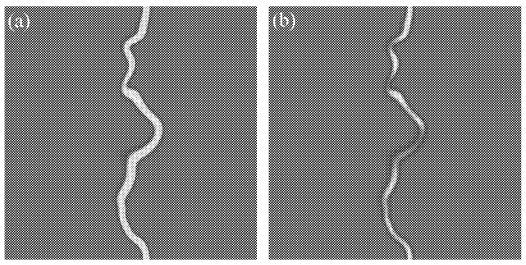

Figure 13: Distributions of heat release rates due to R8 (a) and R9 (b) on a typical cross section.

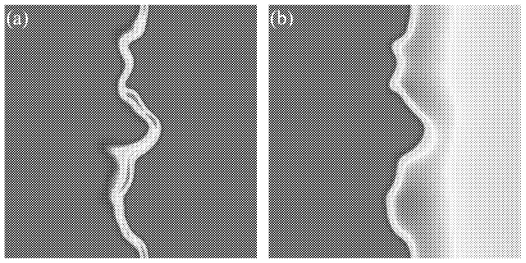

Figure 14: Distributions of mole fractions of CH_3 (a) and O atoms (b) on a typical cross section.

LOCAL EXTINCTION MECHANISM

To clarify the local extinction mechanism, distribution of reactive species and balances of elementary reactions should be considered. Figure 12 shows contributions of dominant elementary reactions to heat release rate in methane-air laminar premixed flames. Elementary reactions in Fig. 12 are as follow;

- R1 : 2O+M $\Leftrightarrow$ O_2+M,
- R5 : H+2O+CH_2O+$N_2$$\Leftrightarrow$ 2OH+NO+HCN,
- R7 : H+2O+C_2H_4+$N_2$$\Leftrightarrow$ OH+CH_3+NO+HCN,
- R8 : H+O+$C_2H_4$$\Leftrightarrow$ H_2+CH_3+CO,
- R9 : O+$CH_3$$\Leftrightarrow$ H+CH_2O.

In this study, balances of the above elementary reactions are investigated carefully. Figure 13 shows distributions of heat release rates due to R8 and R9 on a typical cross section shown in Fig. 6. Although the contribution of heat release rate due to R8 is still high in the low heat release rate region, contribution of R9 is relatively low. Figure 14 shows distributions of mole fractions of reactants in R9; CH_3 and O atoms. The distributions of CH_3 and O atoms are separated into the unburned and burned side of the reaction zone. O atom distribution at the flame front is relatively smooth compared with CH_3 distribution. In Fig. 15, the distributions of

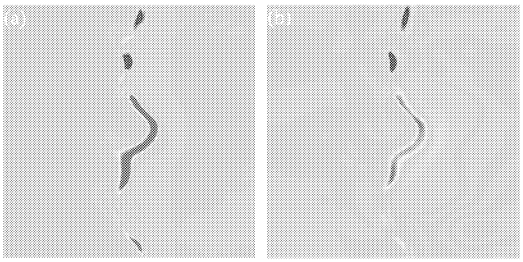

Figure 15: Distributions of reaction rates of CH_3 (a) and O atoms (b) on a typical cross section.

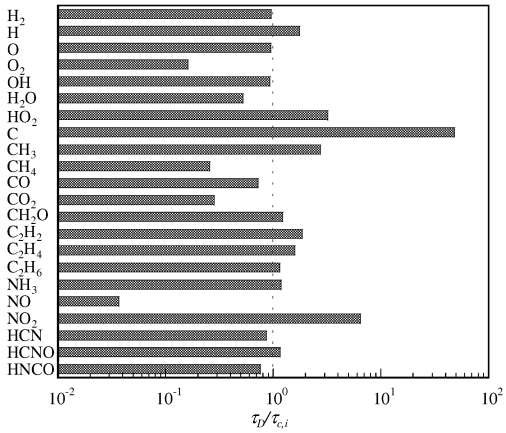

Figure 16: Ratios of lifetimes of species to the eddy turnover time of coherent fine scale eddy.

reaction rates of CH_3 and O atoms are shown. Although the reaction rates of CH_3 and O atoms possesses high values in the low heat release region, they are also separated into the unburned and burned side of the reaction zone.

To clarify the reason why the reactants in R9 are separated, lifetimes of reactive species (Haworth et al., 2000) and an eddy turnover time of coherent fine scale eddy are taken into account. In this study, lifetimes of reactive species are defined as $\tau_{c,i} = [X_i]_{max}/|w_i|_{max}$. $[X_i]_{max}$ and $|w_i|_{max}$ denote the maximum values of molar concentration and reaction rate of specie i in the laminar flame, respectively. An eddy turnover time of coherent fine scale eddy (τ_D) is defined by its most expected diameter (8η) and turbulence intensity (u'_{rms}) because strong coherent fine scale eddies are scaled by u'_{rms}. Figure 16 shows the ratios of lifetimes of reactive species to the eddy turnover time of coherent fine scale eddy. Since the relative lifetime of O atom is close to unity, O atoms are influenced by turbulent velocity field in the unburned side when relatively strong coherent fine scale eddies exist. However, CH_3 can follow the turbulent velocity field. These results suggest that, in highly stretching regions, the effect of convection becomes dominant for distribution of the reactive species which have lifetime close to or less than the eddy turnover time of strong fine scale eddies. On the other hand, the reactive species, which are produced by chain branching reaction of fuel and have large value of $\tau_D/\tau_{c,i}$ like CH_3, are hardly affected by turbulence. Therefore, the reactants of dominant reactions are separated into the unburned side and burned side of the reaction zone. As a result, the dominant reactions are suppressed in highly stretching region.

CONCLUSION

In this study, direct numerical simulation of three-dimensional methane-air turbulent premixed flames propagating in homogeneous isotropic turbulence is conducted to investigate the effects of turbulence characteristics on the local flame structure and the mechanism of local extinction.

In methane-air turbulent premixed flames, local heat release rate is well correlate with tangential strain rate at the flame front. The most expected strain rate is simple two-dimensional stretching of the order of u'_{rms}/λ. The flame elements stretched into two tangential directions shows high heat release rate. However, excessive stretching leads to decrease of the local heat release rate. In contract to hydrogen-air turbulent premixed flames, effects of the flame curvature are not dominant for methane-air flames.

In methane-air turbulent premixed flames, large spots with very low heat release rate are observed. These spots represent local extinction of the premixed flame in turbulence. Flame elements with low heat release rate due to the excessive stretching are observed in the vicinity of these spots. The local extinction mechanism is investigated by introducing lifetime of reactive species relative to eddy turnover time of strong coherent fine scale eddies. Since O atoms cannot follow the strong turbulent motion, one of important elementary reactions for heat release rate ($O+CH_3 \Leftrightarrow H+CH_2O$) is suppressed. This mechanism is well represented by the separation of CH_3 and O reaction rates in the reaction zones.

REFERENCES

Baum, M., Poinsot, T. J., Haworth, D. C. and Darabiha, N., 1994a, "Direct Numerical Simulation of $H_2/O_2/N_2$Flames with Complex Chemistry in Two-dimensional Turbulent Flow," *Journal of Fluid Mechanics*, Vol. 281, pp. 1-32.

Baum, M., Poinsot, T. and Thevenin, D., 1994b, "Accurate Boundary Conditions for Multicomponent Reactive Flows", *Journal of Computational Physics*, Vol. 116, pp. 247-261.

Borghi, R. W., 1985, *Recent Advances in Aeronautical Science*, Plenum, New York, pp. 117.

Bowman, C. T., Hanson, R. K., Davidson, D. F., Gardliner, Jr., W. C., Lissianski, V., Smith, G. P., Golden, D. M., Frenklach, M. and Goldenberg, M., *http://www.me.berkeley.edu/gri_mech*

Chen, J. H., Echekki, T. and Kollmann, W., 1998, "The Mechanism of Two-dimensional Pocket Formulation in Lean Premixed Methane-Air Flames with Implications to Turbulent Combustion," *Combustion and Flame*, Vol. 116, pp. 15-48.

Echekki, T. and Chen, J. H., 1996, "Unsteady Strain Rate and Curvature Effects in Turbulent Premixed Methane-Air Flames," *Combustion and Flame*, Vol. 106, pp. 184-202.

Haworth, D., Blint, R, Poinsot, T. and Cuenot, B., 2000, "Numerical Simulation of Turbulent Propane-Air Combustion with Nonhomogeneous Reactants," *Combustion and Flame*, Vol. 121, pp. 395-417.

Hilbert, R., Tap, F., El-Rabii, H. and Thevenin, D., 2003, "Impact of Detailed Chemistry and Transport Models on Turbulent Combustion Simulations," *Progress in Energy and Combustion Science*, Vol. 30, pp. 61-117.

Homma, R., 2001, "Reduced Mechanism Based on GRI Mech-v2.11 using Quasi-Steady State Assumption" *Proceedings of the Thirty-Nine Japanese Symposium on Combustion*, vol. 39, pp. 533-534.

Kee, R. J., Dixon-Lewis, G., Warnatz, J., Coltrin, M. E. and Miller, J. A., 1986, "A Fortran Computer Code Package for the Evaluation of Gas-Phase Multicomponent Transport Properties", Sandia Report, SAND86-8246.

Kee, R. J., Rupley, F. M. and Miller, J. A., 1989, "Chemkin-II: a Fortran Chemical Kinetics Package for the Analysis of Gas Phase Chemical Kinetics", Sandia Report, SAND89-8009B.

Miller, J. A. and Bowman, C. T., 1989, "Mechanism and Modelling of Nitrogen Chemistry in Combustion", *Progress in Energy and Combustion Science*, vol. 15, pp. 287-338.

Miyauchi, T., Tanahashi, M., Sasaki, K. and Ozeki, T., 1996, "Transport Phenomena in Combustion," Chen, C. H. ed., Taylor and Francis, New York, pp. 1095-1105.

Nada, Y., Tanahashi, M., and Miyauchi, T., 2004a, "Effect of Turbulence Characteristics on Local Flame Structure of H2-Air Premixed Flames," *Journal of Turbulence*, vol. 5, pn. 16.

Nada, Y., Tanahashi, M. and Miyauchi, T., 2004b, "Local Flame Structure of H_2/Air Turbulent Premixed Flames at Different Reynolds Number," *Thermal Science and Engineering*, Vol. 12, pp. 119-120

Peters, N., 1982, "Laminar Flamelet Concepts in Turbulent Combustion," *Proceedings of the Combustion Institute*, Vol. 21, pp. 1231-1250.

Peters, N., 1999, "The Turbulent Burning Velocity for Large-Scale and Small-Scale Turbulence," *Journal of Fluid Mechanics*, Vol. 384, pp. 107-132.

Poinsot, T. J. and Lele, S. K., 1992, "Boundary Conditions for Direct Simulations of Compressible Viscous Flows", *Journal of Computational Physics*, Vol. 101, pp. 104-129.

Poinsot, T. J., Candel, S. and Trouve, A., 1996, "Applications of Direct Numerical Simulation to Premixed Turbulent Combustion," *Progress in Energy and Combustion Science*, Vol. 21, pp. 531-576.

Saito, T., Tanahashi, M. and Miyauchi, T., 2002, "Effects of Turbulence Intensities and Fuel Species in Turbulent Premixed Flames," *Journal of the Combustion Society of Japan*, Vol. 44, pp. 243-252.

Tanahashi, M., Miyauchi,T., Nada, Y. and Imamura, Y., 1998, "Local Flame Structure of a H_2-Air Turbulent Premixed Flame," *Transactions of the Japan Society of Mechanical Engineers B*, Vol. 64, pp. 2662-2668.

Tanahashi, M., Miyauchi, T. and Ikeda, J., 1999, "Identification of Coherent Fine Scale Structure in Turbulence," *Simulation and Identification of Organized Structures in Flows*, Kluwer Academic Publishers, 131.

Tanahashi, M., Fujimura, M. and Miyauchi, T., 2000, "Coherent Fine-Scale Eddies in Turbulent Premixed Flames," *Proceedings of the Combustion Institute*, Vol. 28, pp. 529-535.

Tanahashi, M., Iwase, S., and Miyauchi,T., 2001, "Appearance and alignment with strain rate of coherent fine scale eddies in turbulent mixing layer," *Journal of Turbulence*, vol. 2, pn. 6.

Tanahashi, M., Nada, Y., Ito, Y. and Miyauchi, T., 2002, "Local Flame Structure in the Well-Stirred Reactor Regime," *Proceedings of the Combustion Institute*, Vol. 29, pp. 2041-2049.

Tanahashi, M., Kang, S. -J., Miyamoto, T., Shiokawa, S. and Miyauchi, T., 2004, "Scaling Law of Fine Scale Eddies in Turbulent Channel Flows up to $Re_\tau = 800$," *International Journal of Heat and Fluid Flows*, Vol. 25, pp. 331-340.